Three-dimensional jet tomography of twisted strongly coupled quark qluon plasmas

A. Adil* and M. Gyulassy†
Columbia University, Department of Physics, 538 West 120-th Street, New York, New York 10027, USA
(Received 1 May 2005; published 30 September 2005)

The *triangular* enhancement of the rapidity distribution of hadrons produced in $p+A$ reactions relative to $p+p$ is a leading order in $(A^{1/3}/\log s)$ violation of longitudinal boost invariance at high energies. In $A+A$ reactions this leads to a *trapezoidal* enhancement of the local rapidity density of produced gluons. The local rapidity gradient is proportional to the local participant number asymmetry and leads to an effective rotation in the reaction plane. We propose that three-dimensional jet tomography, correlating the long-range rapidity and azimuthal dependences of the nuclear modification factor $R_{AA}(\eta, \phi, p_\perp; b > 0)$, can be used to look for this intrinsic longitudinal boost violating structure of $A+A$ collisions to image the produced twisted strongly coupled quark gluon plasma. In addition to dipole and elliptic azimuthal moments of R_{AA}, a significant high $p_\perp$ octupole moment is predicted away from midrapidity. The azimuthal angles of maximal opacity and hence minima of R_{AA} are rotated away from the normal to the reaction plane by an octupole twist angle $\theta_3(\eta)$ at forward rapidities.

DOI: 10.1103/PhysRevC.72.034907 PACS number(s): 12.38.Mh, 24.85.+p, 25.75.−q

I. INTRODUCTION

The experimental discovery [1] of a new form of strongly interacting quark gluon plasma matter (called the sQGP [2]) at the Relativistic Heavy Ion Collider (RHIC) has raised many new questions about the physics of ultradense matter produced in relativistic nuclear collisions. Striking new phenomena observed thus far include jet quenching, fine structure of elliptic flow, nuclear gluon saturation, and the baryon-meson anomaly. The primary experimental parameters available at the RHIC are the beam energy, $\sqrt{s} = (20\text{–}200)A$ GeV, and the variation of nuclear geometry through different $B+A$ combinations. Variations of the global nuclear geometry via impact parameter or centrality cuts adds another set of important experimental methods and instruments with which the geometric configuration of the sQGP can be systematically varied. In noncentral collisions of nuclei, the transverse area of the participant interaction region has an elliptic shape with an aspect ratio or eccentricity that can be varied in a controlled way via global multiplicity cuts. In this paper, we explore a more subtle aspects of the three-dimensional (3D) geometry of sQGP produced in noncentral $A+A$ collisions that can be explored by extending jet tomography techniques [3] to full 3D taking the third "slice" dimension to be the rapidity variable.

Strong elliptic transverse flow resulting from transverse elliptic asymmetry provides the key barometric probe of the sQGP equation of state. A common simplifying assumption in most hydrodynamic and transport analyses of the data thus far is that the initial conditions are longitudinally boost invariant [4]. However, the rapidity dependence of elliptic flow data clearly demonstrate important deviations of the global collective dynamics from boost invariance away from the midrapidity region in Refs. [5,6]. Even the most advanced 3+1D hydrodynamic calculations [7–9], which relax the ideal 2+1D Bjorken initial conditions, have not yet been able to reproduce the observed rapidity dependence of elliptic flow. The solution may require better understanding of the geometry of the initial sQGP in addition to better theoretical control over the growing dissipative hadronic corona at high rapidities Ref. [2].

As we show below, the dimensionless parameter that controls violations of longitudinal boost invariance in $A+A$ reactions at finite energies is the *local* relative rapidity slope of the low transverse momentum partons

$$\delta = \frac{A^{1/3} - 1}{2Y}, \tag{1}$$

where $2Y = \log s$ is the rapidity gap between the projectile and target. In Au+Au at RHIC $\sqrt{s} = 200A$ GeV, $\delta \approx 0.45$ cannot be ignored. Even in Pb+Pb at the Large Hadron Collider (LHC) $\sqrt{s} = 5500A$ GeV, $\delta \approx 0.28$ will not be much smaller.

In this paper, we explore some observable consequences of such violations of longitudinal boost invariance. We predict that there is an intrinsic rotation of the initially produced matter in the reaction plane in noncentral $A+A$ that can induce an octupole moment of the nuclear modification factor $R_{AA}(\eta \neq 0, \phi, p_\perp; b > 0)$ at moderate to high $p_\perp$ away from midrapidities. This effect arises from the combination of two basic properties of high-energy hadron-nucleus reactions with jet quenching dynamics in $A+A$.

One important property is that the rapidity density of produced hadrons is observed [10] to be *triangular* relative to the density produced in $p+p$ reactions with a slope given by $\sim\delta$. The second basic property follows from the eikonal Glauber reaction geometry that predicts *local* variations of the projectile and target participant number density in the transverse plane $\mathbf{x}_\perp$. We propose that the long-range correlations of the rapidity and azimuthal dependence of jet quenching can be used to extend current 2D $R_{AA}(\phi)$ jet tomography Ref. [3] to "image" the 3D geometry of the twisted sQGP initial state at forward rapidities $|\eta| \sim 1\text{–}3$.

In the next section, we begin with a review of the $p+A$ triangle and its implications for $A+A$ initial conditions. In Sec. III, we discuss the role of more realistic diffuse

*Electronic address: azfar@phys.columbia.edu
†Electronic address: gyulassy@phys.columbia.edu

nuclear geometry on the local participant and binary collision densities. In Sec. IV, we calculate jet opacities as a function of η, ϕ. In Sec. V, jet attenuation through the tilted bulk sQGP density in the reaction plane is studied, and in Sec. VI, the azimuthal Fourier moments of the nuclear modification factor are computed as a function of rapidity. Our proposed new observable, the octupole twist angle $\theta_3(\eta)$, is computed. We conclude in Sec. VII.

II. THE $p + A$ TRIANGLE

In $p+A$ reactions, the ratio $R_{pA}(\eta) = (dN_{pA}/d\eta)/(dN_{pp}/d\eta)$ of produced low $p_\perp$ hadrons as a function of rapidity η was found at all energies to be "triangular" with the height near the rapidity $(-Y)$ of the target nucleus proportional to $\nu_A \propto A^{1/3}$, the average number of "wounded target nucleons" Refs. [10,11]. (Note that we are using the variable η to denote the particle rapidity rather than the particle pseudorapidity, to which η is conventionally linked. This is to avoid later confusion with the variable y used in this paper to denote the transverse vertical coordinate.) Excess nuclear enhancement $\propto A^{1/3+q}$ near the target rapidity is due to intranuclear cascading of low relative energy hadrons produced in the target fragmentation region. We will not consider this extra nuclear modification further in this paper.

The projectile proton in the center of rapidity frame has rapidity Y and interacts at a transverse impact parameter $\mathbf{b}$ on the average with

$$\nu_A(\mathbf{b}) \approx \sigma_{\rm in} T_A(\mathbf{b}) = \sigma_{\rm in} \int dz\, \rho_A(z, \mathbf{b}) \propto A^{1/3} \qquad (2)$$

target nucleons with rapidity $-Y$. Here $\sigma_{\rm in}(\sqrt{s})$ is the NN inelastic cross section, and the Glauber profile function $T_A(\mathbf{b})$ measures the number target nucleons per unit area of nucleus with proper density $\rho_A(r)$.

The simplest way to understand the origin of the pA triangle is in terms of phenomenological string models of high-energy inelastic interactions. Each wounded nucleon [11] in both projectile and target is diffractively excited into high mass $\sim\sqrt{s}/2$ states that decay as beam jets into relatively low transverse momentum ($p_T \sim \Lambda_{\rm QCD}$) over a wide rapidity interval. Wounded target nucleons decay over an interval $-Y < \eta \lesssim 0$, while projectile nucleons decay over $0 \gtrsim \eta < Y$. The resulting asymmetry of the produced hadron rapidity density $dN_{pA}/d\eta$ thus grows approximately linearly with ν_A.

At RHIC [12], the rapidity triangle was clearly observed in the deuterium+Au control experiment at 200A GeV relative to pp and $p\bar{p}$ [13] as shown in Fig. 1. The absolute agreement between HIJING calculations and the measured multiplicities can be seen in Fig. 2. The disagreement between experiment and theory at extreme negative rapidities marks the presence of intranuclear cascading. Also note that the figures show pseudorapidity distributions rather than rapidity distributions. These are the same up to a Jacobian suppression factor present in all pseudorapidity distributions (15%), which can be seen in Fig. 1. This Jacobian factor cancels in the ratio.

One of the early parton model interpretations of the rapidity triangle and its generalization to rapidity "trapezoids" in $B+A$ collisions was given in Brodsky, Gunion, and Kuhn (BGK) [16]. The color excitation of wounded baryons proceeds in this picture with a parton-parton scattering at a rapidity, y^* distributed approximately uniformly between $-Y$ and Y. The color excited projectile nucleon then neutralizes by producing a string of hadrons from $y^* < \eta < Y$, while the target nucleon neutralizes by producing a string of hadrons from $-Y < \eta < y^*$. The approximately triangular rapidity density in this model arises naturally from the sum over the ν_A target and one projectile fragments.

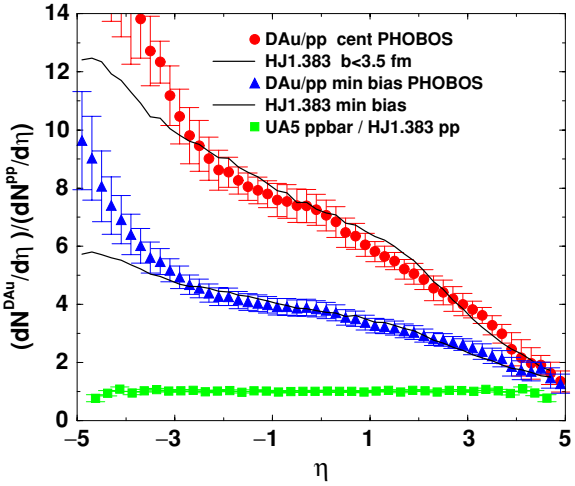

FIG. 1. (Color online) Approximate triangular form of the ratio of the observed D+Au [12] charged particle pseudorapidity distributions to the dashed HIJING $p+p$ curve from Fig. 1 are shown for two centrality cuts. Solid curves are predictions using HIJING 1.383 [14,15] for D+Au/$p+p$. The ratio of UA5 $p+\bar{p}$ [13] data to the baseline HIJING $p+p$ predictions are shown by filled squares.

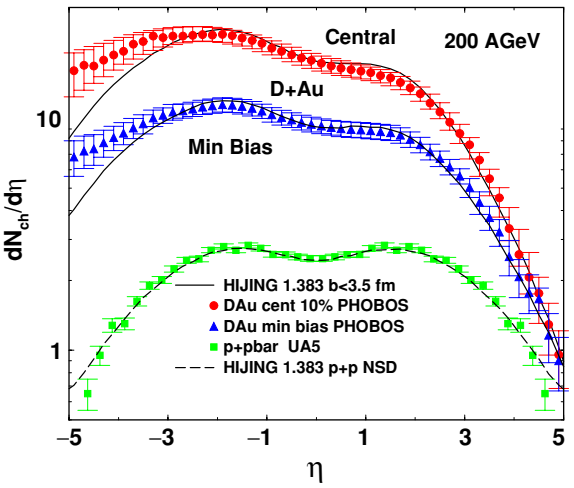

FIG. 2. (Color online) Asymmetric pseudorapidity distributions of charged hadrons produced in D+Au minimum bias and central 0–10% reactions at 200A GeV from PHOBOS [12] are compared to $p+\bar{p}$ data from UA5 [13]. The curves show predictions using the HIJING v1.383 code [14,15].

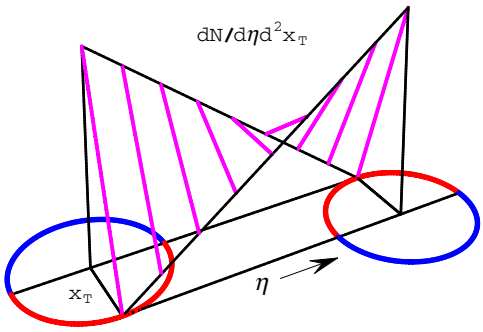

FIG. 3. (Color online) Schematic illustration of how local trapezoidal nuclear enhancements of the rapidity distributions in the reaction plane $(x, \eta, y = 0)$ twist the bulk initial density about the normal in noncentral $A+A$ collisions. See Eqs. (3) and (8).

BGK [16] generalized this model to predict the "trapezoidal" distributions that would arise when a row of $\nu_B > 1$ projectile nucleons interacts inelastically with a row of $\nu_A > 1$ target nucleons. This very basic feature of multinucleon interactions in pQCD is at the core of the phenomenological success of LUND string models such as FRITIOF [17] and HIJING [14,15]. The curves shown in Figs. 1 and 2 are predictions of the HIJING model [15] using version 1.383, which includes the Hulthen distribution of nucleons in deuterium. The magnitude and centrality dependence of the charged particle rapidity distributions are well predicted by the basic trapezoidal nuclear enhancement of multiparticle production dynamics. We note that Wang [18] studied this rapidity asymmetry also as a function of p_T out to moderately high $p_\perp$ to test Cronin versus shadowing dynamics away from midrapidity.

While the *global* features of the $p_\perp$ integrated $dN/d\eta$ are well accounted for, we focus in this paper on the novel *local* implications of the trapezoidal violations of longitudinal boost invariance for the initial conditions in $B+A$. In a noncentral collision at an impact parameter $\mathbf{b}$, the *local* enhancement of bulk particle production relative to $p+p$ at a particular transverse coordinate $\mathbf{x}_\perp$ is approximately given in the BGK model by

$$\frac{dR_{BA}}{d^2\mathbf{x}_\perp}(\eta, \mathbf{x}_\perp; \mathbf{b}) = \frac{dN^{BA}/d\eta d^2\mathbf{x}_\perp}{dN^{pp}/d\eta} \approx \nu_A(\mathbf{x}_\perp - \mathbf{b}/2)\frac{Y-\eta}{2Y} + \nu_B(\mathbf{x}_\perp + \mathbf{b}/2)\frac{Y+\eta}{2Y}. \quad (3)$$

Even if $p+p$ were longitudinally boost invariant with a constant $dN^{pp}/d\eta$, the variation of ν_A and ν_B with $\mathbf{x}_\perp$ leads to local violations of longitudinal boost invariance in noncentral $B+A$. The local deviations are controlled by

$$\delta(\mathbf{x}_\perp; \mathbf{b}) = \frac{\nu_B - \nu_A}{2Y}, \quad (4)$$

i.e., the local participant asymmetry $\nu_T - \nu_P$ at $\mathbf{x}_\perp$.

For very large energies, $Y \gg 1$, Bjorken longitudinal boost invariance is restored. However, for Au+Au at RHIC, $Y \approx 5$, $A^{1/3} \sim 6$, and there is an order unity variation of δ across the transverse profile of the interaction region that leads to the twisted ribbon geometry of the local density distribution as illustrated schematically in Figs. 3 and 4. In these figures, the coordinate normal to the reaction plane y, is set to zero, and the surface dR_{AA} is illustrated as a function of $x = x_T$ in different η slices. In reality, only the fixed x slices have trapezoidal shape while the η slices are rounded because of the nonlinear dependence of ν_i on transverse coordinates.

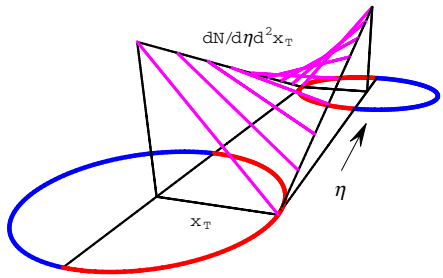

FIG. 4. (Color online) As in Fig. 3 from another perspective. The straight segments in each rapidity slice are for emphasis only. Realistic diffuse spherical geometries curve these lines (see Fig. 7 below).

At the global $dN/d\eta$ level, integration over the transverse coordinates leads to

$$R_{BA}(\eta; \mathbf{b}) = \frac{dN^{BA}/d\eta}{dN^{pp}/d\eta} \approx \frac{1}{2}(N_A + N_B) + \frac{\eta}{2Y}(N_B - N_A), \quad (5)$$

where $N_A = \int d^2\mathbf{x}_\perp \nu_A(\mathbf{x}_\perp; \mathbf{b})$ and N_B are the total number of wounded target and projectile nucleons interacting at impact parameter b. What is remarkable about Eqs (3) and (5) and readily seen on in Figs. 3 and 4 is that for *symmetric* $A+A$ reactions, the global ratio may appear to be approximately boost invariant, but the local density retains an *intrinsic* rapidity asymmetry that can be characterized by a rotation twist in reaction plane

$$T_{x\eta} = \frac{\partial^2}{\partial\eta\partial x}\log\left(\frac{dN}{d\eta d^2\mathbf{x}_\perp}\right), \quad (6)$$

where x and y are the coordinates in and out of the reaction plane. A useful property of this characterization is that it is independent of the normalization of dN and independent of the multiplicative rapidity modulation factor $dN^{pp}/d\eta$.

For a sharp sphere geometry with

$$\nu \propto \sqrt{R^2 - (x \pm b/2)^2 - y^2}, \quad (7)$$

the $x\eta$ twist in the center $x = y = 0$ of the oval interaction region is independent of η and given by

$$T_{x\eta}(\mathbf{x}_\perp = 0) = \frac{1}{Y}\frac{2b}{4R^2 - b^2}. \quad (8)$$

The twist would of course be absent if nuclei were uniformly thick. The magnitude for realistic spherical nuclei depends on the actual diffuse Woods-Saxon geometry that we use for our numerical estimate below. However, (8) shows that its typical magnitude of $T_{x\eta}$ is $1/(RY)$ in minimum bias reactions.

We also note that the trapezoidal distribution of low p_T multiparticle production in D+Au follows more generally if the collinear factorized QCD minijet dynamics of BGK is replaced by the k_T factorized gluon fusion mechanism

in the color glass condensate (CGC) model Refs. [19,20]. Quantitative differences between these mechanisms arise at moderate $p_T > 2$–5 GeV, which are currently under investigation at RHIC [1,21]. They are connected with different physical approximations to Cronin enhancement and gluon shadowing Ref. [22].

The empirical trapezoidal form (3) in both BGK and CGC cases differs from local equilibrium initial conditions based on firetube or firestreak models [7,9,23]. While such models also predict an effective tilt in the $x\eta$ plane, they correspond to possible initial rapidity shear of the hydrodynamic fluid at fixed η. In our approach, there is no initial rapidity shear, and the collective longitudinal "fluid" velocity vanishes in the comoving ($y = \eta$) frame over the whole transverse region. However, there is an initial gradient of the density along the beam axis that can induce a fluid shear during later evolution. Polarization has been proposed as an observable sensitive to rapidity shear [24]. We concentrate here on generic trapezoidal (BGK, HIJING, or CGC) initial twisted sQGP conditions because they follow directly from QCD parton dynamics and are well constrained by $p+A$ phenomenology.

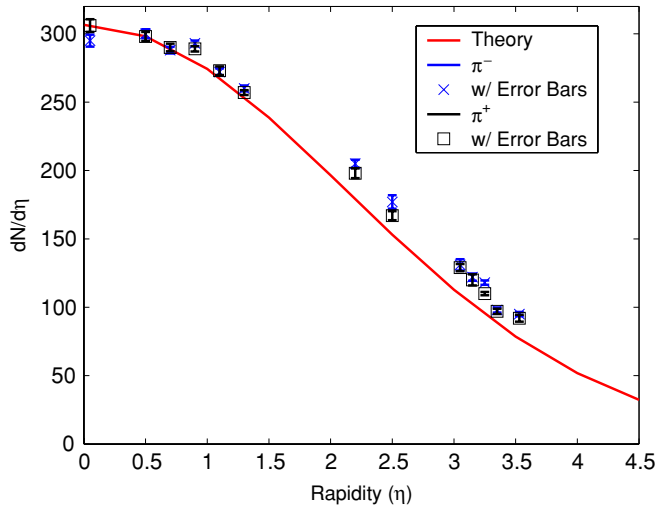

FIG. 5. (Color online) A Gaussian fit of the $\pi^{\pm}$ rapidity density in central Au+Au at 200A GeV is shown compared to BRAHMS [25] data.

III. DIFFUSE NUCLEAR GEOMETRY

To take the diffuse nuclear geometry into account, we recall that the local projectile B and target A participant densities are given in Glauber theory by

$$\frac{dN^B_{\rm part}}{dxdy} = T_B(r_+)(1 - e^{-\sigma_{\rm in} T_A(r_-)})$$
$$\frac{dN^A_{\rm part}}{dxdy} = T_A(r_-)(1 - e^{-\sigma_{\rm in} T_B(r_+)}), \qquad (9)$$

where $r_\pm = \sqrt{(x \pm \frac{b}{2})^2 + y^2}$ and $\sigma \approx 42$ mb at $\sqrt{s} = 200A$ GeV. Rare jets are produced, on the other hand, distributed in the transverse plane according to the binary collision number distribution given by

$$\frac{dN_{\rm Bin}}{dxdy} = \sigma_H T_B(r_+) T_A(r_-), \qquad (10)$$

where $\sigma_H(p_\perp, \eta)$ is the pQCD jet cross section. For $B = A$ collisions, the binary distribution is obviously symmetric in the transverse plane at any impact parameter, unlike the participant distributions. Nuclear shadowing and Cronin effects can break this symmetry; but for the present study, we assume that at high enough p_T, these initial state nuclear effects can be neglected.

Jet quenching at a given rapidity in azimuthal direction ϕ depends on a transverse coordinate line integral across the sQGP density profile at that rapidity [3]. The initial sQGP density is assumed here to be proportional to the local participant density. In the BGK model, this is then approximately given by

$$\frac{dN_g}{dxdyd\eta} = \frac{C}{2Y} \exp\left[\frac{-\eta^2}{\sigma_\eta^2}\right] \theta(Y - |\eta|)$$
$$\times \left\{ \frac{dN^A_{\rm Part}}{dxdy}(Y - \eta) + \frac{dN^B_{\rm Part}}{dxdy}(Y + \eta) \right\}, \qquad (11)$$

where we have introduced a Gaussian rapidity envelope to model $dN^{pp}/d\eta$ at RHIC. With $Y = 5$, $\sigma_\eta = 3$, and $C \approx 24$, the $\mathbf{x}_\perp$ integrated $dN_g/d\eta \times 1/3$ fits the BRAHMS central Au+Au$\rightarrow \pi^+, \pi^-$) data [25] as shown in Fig. 5.

Figures 6 and 7 show the 3D diffuse participant geometry of the twisted sQGP initial conditions (11) in the transverse plane in several impact parameter and rapidity slices. For $b = 0$, there is complete azimuthal symmetry at all rapidities, of course. For finite b, the initial sQGP density shifts to the left at forward rapidities and to the right in backward rapidities with our conventions. The shifts are small < 2 fm, but distinct. There is also a small increase in the eccentricity, $\epsilon(\eta) = \langle (x - \langle x \rangle)^2 - y^2 \rangle / \langle (x - \langle x \rangle)^2 + y^2 \rangle$, of the twisted sQGP density away from midrapidity as shown in Fig. 8.

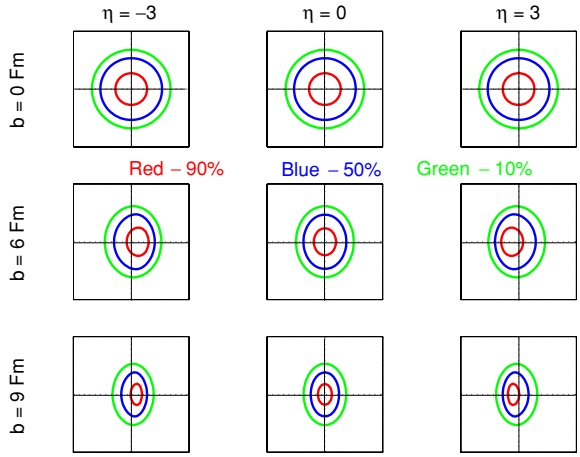

FIG. 6. (Color online) Contours of the twisted sQGP initial density in the transverse plane (x, y) in different rapidity $\eta = -3, 0, 3$ and impact parameter $b = 0, 6, 9$ fm slices. Note the opposite transverse shifts at η and $-\eta$.

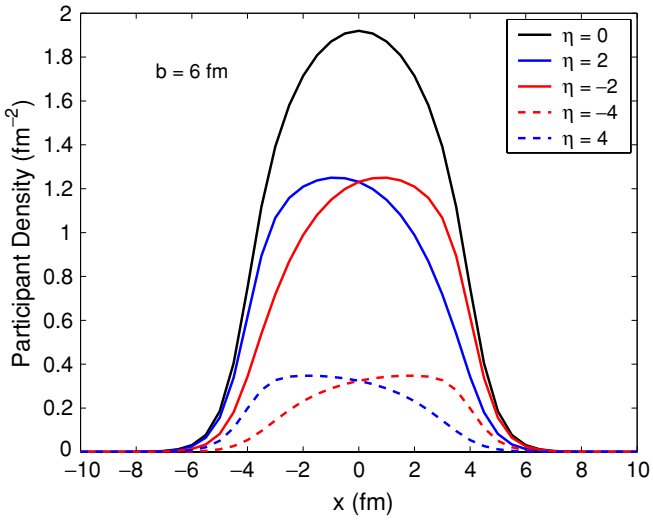

FIG. 7. (Color online) Transverse profile of the twisted sQGP at $b = 6$ fm as a function of transverse coordinate x at $y = 0$ for $\eta = \pm 2, \pm 4$. The normalization is to the local transverse participant density fm^{-2}. The overall decrease of the density away from midrapidity is due to the approximate Gaussian envelope in Fig. 5.

IV. AZIMUTHAL DEPENDENCE OF THE TWISTED sQGP OPACITY

Unlike the participant scaling bulk sQGP density, the binary jet distribution (10) does not manifest a rapidity asymmetry at least at enough high p_T where shadowing is expected to be small. The jet production points are therefore not rotated away from the beam direction in this limit. This is illustrated in Fig. 9.

Jet quenching due to energy loss in the medium depends on the opacity and hence density of the plasma in the direction of propagation [3,26]. The mismatch between the distribution of jet production points and the rotated distribution of the

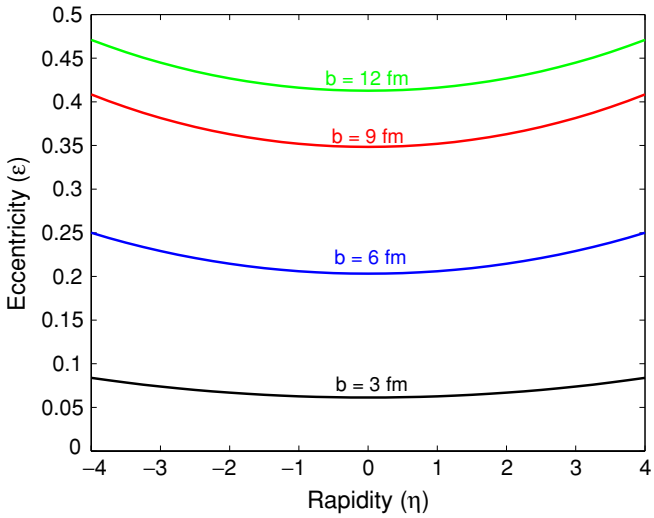

FIG. 8. (Color online) Rapidity dependence of the elliptic eccentricity of the twisted sQGP.

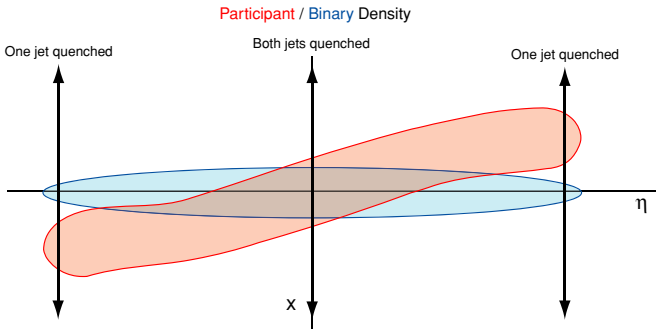

FIG. 9. (Color online) Schematic illustration of the orientation of the initial twisted sQGP (11) relative to the symmetric binary collision distribution (10) of jet production points projected onto the (x, η) reaction plane. The extra azimuthal asymmetry and octupole twist of jet quenching results from the relative rotation of these two distributions.

bulk sQGP matter therefore induces a peculiar azimuthal dependence of the weighed opacity such that

$$\chi_\alpha(x_0, y_0, \eta, \phi, b) = c_\alpha \int_{\tau_0}^{\infty} dt\ t^\alpha \frac{dN_g}{dx dy d\eta} \times [x_0 + t\cos(\phi), y_0 + t\sin(\phi), b]. \tag{12}$$

Different $\alpha = -1, 0, 1$ weights correspond to different mechanisms of energy loss. Elastic scattering energy loss through longitudinally expanding [4] (or static) sQGP matter corresponds to $\alpha = -1$ (0). Inelastic radiative energy loss through longitudinally Bjorken expanding (or static) sQGP matter corresponds, on the other hand, to $\alpha = 0$ (1). The results turned out numerically to be within 10% in all cases. Therefore, from now on, we drop the α index and show results only for $\alpha = 0$.

We show in Figs. 10 and 11 the ϕ dependence of the opacity for different b and η. In all cases, the opacity is normalized to the maximal $x_0 = y_0 = b = \eta = 0$ opacity

$$\chi_0 \equiv \chi_0(0, 0, 0, 0). \tag{13}$$

In Fig. 10, $\chi_0(0, 0, \eta, \phi)/\chi_0$ is shown for a jet produced at the origin $x = y = 0$ for $b = 3, 6, 9$ fm. For each b, we consider the azimuthal variation at $\eta = 0, \pm 2, \pm 4$. First, note that the magnitude of the opacity is proportional to the decreasing central density as either b or $|\eta|$ increases. Second, the amplitude of the elliptic second moment $\langle\cos(2\phi)\rangle$ increases as the eccentricity of the sQGP increases, with b, as seen in Fig. 8. Third, the maximum opacity at $\eta = 0$ is in directions perpendicular to the impact parameter vector (where there is more matter) and minimum in directions parallel to it. These features and trends are the familiar ones in the conventional standard Bjorken scenario [26].

However, the new twists caused by the intrinsic longitudinal boost violating $\delta = O(1)$ initial conditions illustrated in Fig. 9 are (1) the emergence of a long-range rapidity asymmetry between $+\eta$ and $-\eta$ with a 180° phase shifted azimuthal dependence and (2) an azimuthal pattern that has odd harmonics in addition to quadrapole $v_2 = \cos(2\phi)$ moment. It is clear that there is a significant high p_T $v_1 = \cos(\phi)$ dipole moment away

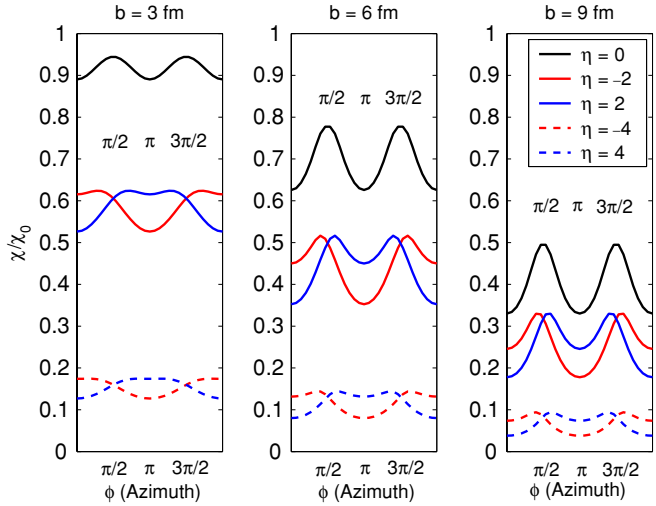

FIG. 10. (Color online) Opacity χ as a function of azimuthal angle ϕ for different values of rapidity and impact parameter. The jet is assumed to be born at the origin of the transverse plane. The functions have been normalized to χ_0, the opacity felt by a jet propagating along the x axis after being born at the origin of the transverse plane, at midrapidity, and with impact parameter zero.

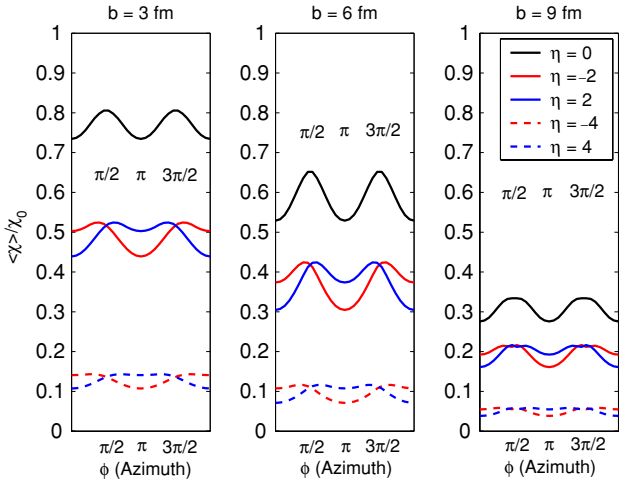

FIG. 11. (Color online) Averaged opacity χ as a function of azimuthal angle ϕ for different values of rapidity and impact parameter. The initial position of the jet seeing the opacity is averaged over the binary distribution. The functions have been normalized to χ_0, the opacity felt by a jet propagating along the x axis after being born at the origin of the transverse plane, at midrapidity, and with impact parameter zero.

from midrapidity. This is manifest in the difference between $\chi(\phi = 0, \eta)$ and $\chi(\pi, \eta)$ as expected from Fig. 9.

The most interesting new and subtle feature in Fig. 10 however, is that the azimuthal angles of maximum opacity for $\eta \neq 0$ are no longer at $\phi = \pi/2$ and $3\pi/2$, as at $\eta = 0$, but rotated slightly away from the normal to the reaction plane.

The splitting of the maxima is the unique new signature of the Bjorken violating initial conditions considered here. Both v_1 and v_2 at high rapidities are well known and expected in nuclear collisions because of the directed and elliptic hydrodynamic flow of the bulk matter (see Stoecker [2,27]). However, the long-range rapidity anticorrelation of the azimuthal rotation of opacity maxima, which as we show below correspond to jet quenching minima, is the smoking gun that we propose as the test of twisted sQGP initial conditions.

To test the robustness of this signal, we next average over all the initial jet production points using the binary collision number distribution

$$\langle \chi \rangle = \frac{1}{dN_{\rm Bin}/d\eta} \int dx_0 dy_0 \frac{dN_{\rm Bin}}{dx dy d\eta}(x_0, y_0, b)\chi. \qquad (14)$$

The results shown in Fig. 11 show all the same qualitative effects as seen in the center jet results in Fig. 10, but they are slightly diluted because of the extra averaging over $\mathbf{x}_0$.

In the case that we consider here, the relatively normalized $dN_{\rm Bin}$ actually has no η dependence. At moderate p_T, the interplay between Cronin and shadowing could give rise to an η dependence which we will report in a subsequent paper.

V. AZIMUTHAL DEPENDENCE OF R_{AA}

The observation of jet quenching in different η slices makes it possible to extend 2D jet tomography to 3D. The observable is the nuclear modification factor

$$R_{AA} = \frac{dN_{AA}/d\eta d^2 p_T}{T_{AA} d\sigma_{pp}/d\eta d^2 p_T}. \qquad (15)$$

This is the ratio between the spectrum of high p_T hadrons produced in $A+A$ and the inclusive differential cross section in proton-proton collisions scaled by the binary transverse density, $T_{AA}(b) = \int d^2\mathbf{x} T_A(r_+) T_A(r_-) = N_{\rm Bin}(b)/\sigma_H$.

In general, the computation of $R_{AA}(\eta, \phi, p_\perp)$ requires averaging over the power law pQCD parton spectra, using the distribution of energy loss as in the Gyulassy-Levai-Vitev (GLV) or Baier-Dokshitzer-Mueller-Schiff (BDMS) theory [3], and integrating over hadron fragmentation functions. This is beyond the scope of the present paper. Since our aim here is mainly to introduce and illustrate the qualitative features of twisted sQGP initial conditions, the simple phenomenological jet absorption model used in Ref. [28] will suffice for our purposes. In this model, the survival of a jet in direction ϕ relative to the reaction plane is simply assumed to be $\exp[-\kappa\chi(\phi)]$. Averaging over the production points and taking into account the particular geometric dependence of the line integral for opacity (12) for our geometry, the nuclear modification factor is given by

$$R_{AA}(\eta, \phi; b) = \frac{1}{N_{\rm Bin}} \int d^2\mathbf{x}_0 \frac{dN_{\rm Bin}}{d^2 x}(\mathbf{x}_0, b) e^{-\kappa\chi(\mathbf{x}_0, \eta, \phi, b)}. \qquad (16)$$

We simplify the computation of κ by simply fitting the observed [1] approximately p_T independent central collision $R_{AA} \approx 0.2$ in Au+Au at $\sqrt{s} = 200A$ GeV. (This is achieved if $\kappa \approx 0.25$ in units where the central opacity for $b = 0$ is $\chi_0 = 11/\text{fm}^2$).

The computed jet survival probability R_{AA} as a function of azimuthal angle for different rapidities and impact parameters

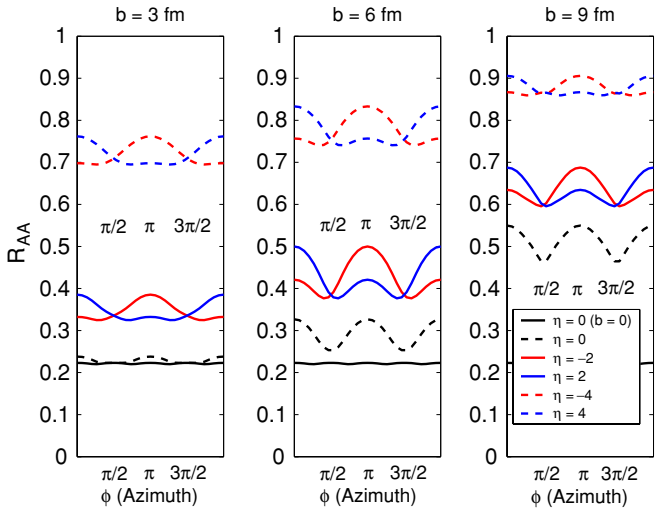

FIG. 12. (Color online) The jet survival probability R_{AA} as a function of azimuthal angle ϕ for different values of rapidity and impact parameter. Note the shifted minima of R_{AA} for $\eta = \pm 2$ near $\phi = \frac{\pi}{2}, \frac{3\pi}{2}$ and the overall π phases shift characteristic of the twisted sQGP initial conditions as in Figs. 10 and 11.

can be seen in Fig. 12. The solid black line in the figure is the $R_{AA} = 0.2$ independent of ϕ is baseline fit for $\eta, b = 0$. The main features to note are the same as in Figs. 10 and 11 but with opacity maxima replaced by slightly shifted R_{AA} minima. First, the magnitude of R_{AA} increases with both increasing impact parameter as well as η. Next, note that at midrapidity, $\eta = 0$, there is a symmetry between $\phi = 0$ and $\phi = \pi$ as usual. The elliptic distribution at $b > 0$ but $\eta = 0$ leads to the usual minimum of the survival probability at $\phi = \pi/2, 3\pi/2$.

However, the reflection symmetry is broken away from midrapidity because the jet source and bulk sQGP are shifted relative to each other. As expected from Figs. 10 and 11, the minimum survival probability is rotated away from the reaction plane normal in opposite directions in the forward and backward rapidity region. To better quantify this effect, we introduce in the next section the octupole twist observable.

VI. THE OCTUPOLE TWIST AND FOURIER DECOMPOSITION

One way to visualize the azimuthal asymmetry of R_{AA} is to compare the jet survival probability in forward and backward rapidity on the same polar plot as shown in Fig. 13. For each fixed rapidity slice and impact parameter, we normalize $R_{AA}(\eta, \phi; b)$ by its minimum $R_{AA}^{\min}$ over ϕ and plot the resulting $R_{AA}/R_{AA}^{\min}$ as a function of ϕ.

For $b = 0$ collisions, this relatively normalized ratio is a unit circle independent of ϕ and η. It is shown as a thin circle. For $b > 0$ but $\eta = 0$, the transverse density profile has an elliptic shape centered at $x = y = 0$, with its longest axis oriented normal to the reaction plane as seen in Fig. 9. This leads to the highest survival probability in the reaction plane $\phi = 0, \pi$, as shown by the thick solid black line in Fig. 13.

For both $b > 0$ and $\eta > 0$, the bulk matter is shifted toward $\phi = \pi$ (in our conventions) leading to a smaller survival probability than in the $\phi = 0$ direction as shown by the solid

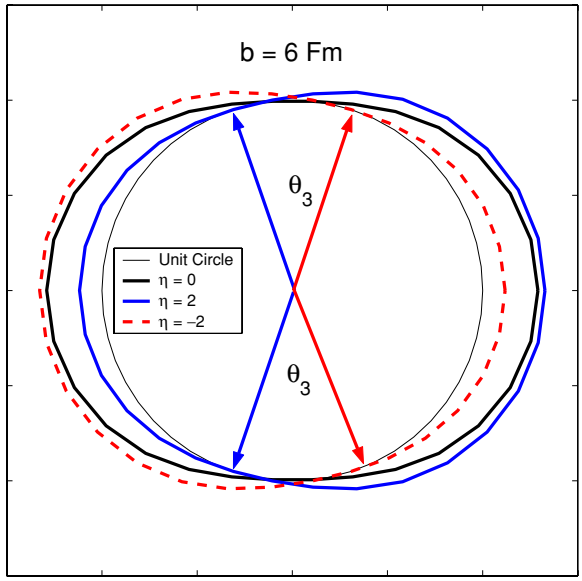

FIG. 13. (Color online) Polar plot of the relatively normalized $R_{AA}/R_{AA}^{\min}$ for $b = 6$ comparing two $\eta = \pm 2$ slices (blue solid, dashed red) to the unit circle corresponding to $b = 0$ (thin black). For $b = 6$ but $\eta = 0$ (thick black), the minima are at $\phi = \frac{\pi}{2}, \frac{3\pi}{2}$ and maxima are at $\phi = 0, \pi$. However, for both $b > 0$ and $|\eta| > 0$, twisted sQGP initial conditions lead to an octupole "pear" deformation with the minima shifted to $\phi = \frac{\pi}{2} + \frac{\theta_3}{2}, \frac{3\pi}{2} - \frac{\theta_3}{2}$. The octupole twist angle $\theta_3(\eta)$ is a measure of the long range in rapidity correlations caused by intrinsic local $O(A^{1/3}/Y)$ violations of longitudinal boost invariance in $A+A$.

(blue shifted) pear shape curve in the figure. The long-range twisted sQGP initial conditions lead on the other hand for $\eta = -|\eta| < 0$ to an azimuthal pattern (red shifted dashed) that is simply the reflected version of the $\eta > 0$ curve about the y axis. The pair of minima of both curves are indicated by the arrows.

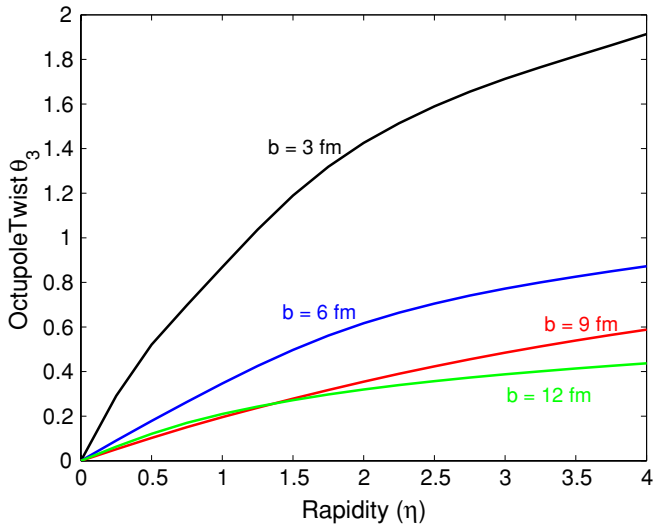

FIG. 14. (Color online) Octupole twist angle $\theta_3(\eta)$ of the minimum jet survival direction as in Fig. 13 for different values of the impact parameter.

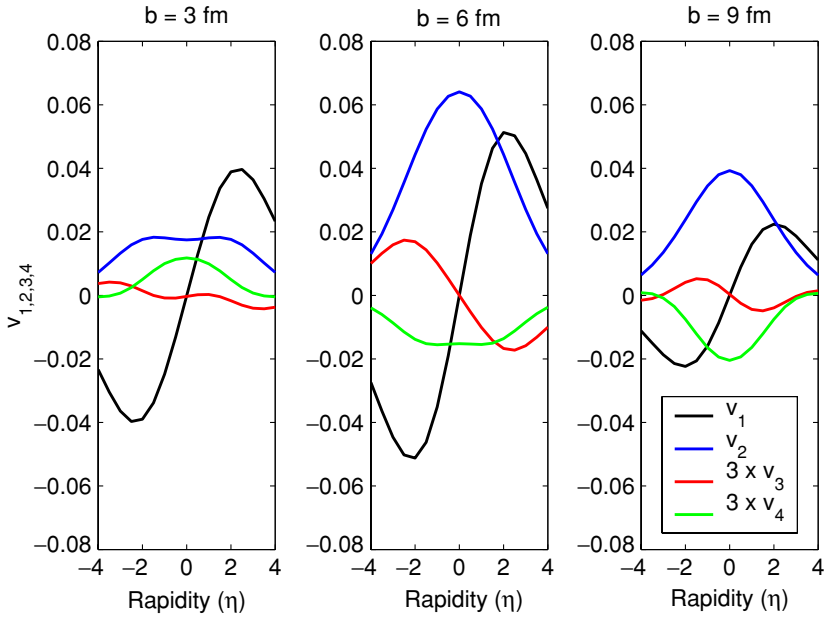

FIG. 15. (Color online) Fourier moments of R_{AA} against rapidity for different values of the impact parameter. Note that the third and fourth moments are shown multiplied by 3.

We define an "octupole twist" angle $\theta_3(\eta, b)$ to help quantify the magnitude of these long-range rapidity correlations as

$$\theta_3(\eta, b) = \phi\big[R_{AA}^{\min}(\eta, b)\big] - \phi\big[R_{AA}^{\min}(-\eta, b)\big]. \qquad (17)$$

The minima in the forward region are tilted to $(\pi - \theta_3)/2$ and $(3\pi + \theta_3)/2$, while in the backward region they are tilted in the opposite direction (Fig. 14).

Note that the reaction plane orientation can be unambiguously determined experimentally via standard low p_T bulk directed and elliptic flow v_1, v_2 [6]. Jet tomography of high p_T hadrons provides a complementary short wavelength probe of the reaction dynamics and can also be decomposed into azimuthal harmonics as

$$R_{AA}(\eta, \phi, p_\perp; b) = a\Big[1 + 2\sum_n v_n \cos(n\phi)\Big]. \qquad (18)$$

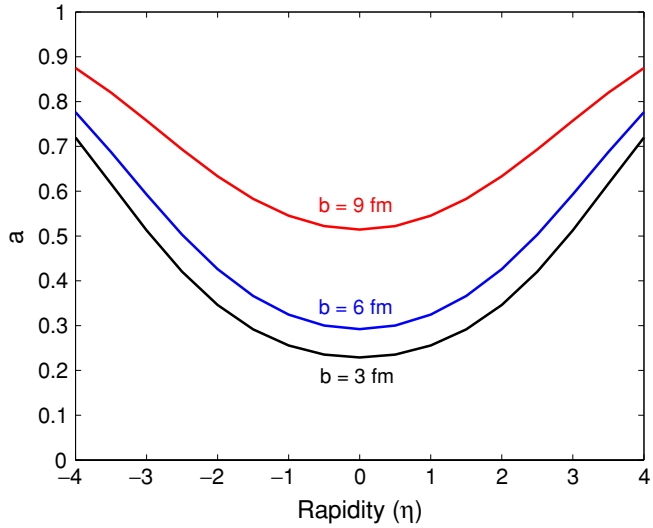

FIG. 16. (Color online) $a(\eta, b)$ vs η for different values of the impact parameter.

The numerical evaluation of the first four moments, $v_n(\eta, b)$, are shown in Figs. 15 and 16. In addition to the usual v_1, v_2 and even v_4 moments, the new feature shown here is the existence of an octupole $v_3 = \langle\cos(3\phi)\rangle$ harmonic that is responsible for the pear shape deformation of R_{AA} in Fig. 13. The magnitude is relatively small, though, on the order of v_4. However, v_4 for low p_T has already been successfully measured [6], and with a large luminosity upgrade and advanced detectors, a measurement of v_3 at $\eta = \pm 2$ may thus become possible at a future RHIC II [29].

The predicted peak of the high p_T $|v_1|$ at $\eta \sim 2$ (with opposite sign relative to the spectator v_1) is another characteristic feature that can be used to test twisted sQGP initial conditions via 3D jet tomography.

VII. CONCLUSIONS

In this paper, we applied the local trapezoidal multiparticle production BGK model to predict the magnitude of intrinsic longitudinal boost violating features of the bulk matter produced in $A+A$ collisions. We noted that this is a generic feature of both local minijet-based dynamics as encoded in LUND string and HIJING models as well as k_T factorized production models such as the CGC. The resulting geometrical picture is that the sQGP initial conditions has the expected transverse elliptical shape for noncentral collisions, but the bulk density is twisted away from the beam axis in the reaction (x, η) plane.

In contrast, the binary collision distribution of hard pQCD jet sources remains reflection symmetric in the transverse plane oriented parallel to the beam axis at least in the approximation that Cronin and shadowing can be neglected at high enough p_T. These approximations will be relaxed in a subsequent paper to explore further how the p_T-dependent 3D jet tomography of twisted sQGP initial conditions can be used to further test different models of gluon saturation.

The generic displacement of the jet sources and bulk matter away from central rapidities was predicted to produce a novel jet absorption pattern that deviates from what is now known at midrapidities. The most intriguing is the predicted octupole twist of the minimum of R_{AA} away from the normal of the reaction plane and a peak of the jet v_1 near $\eta \sim \pm 2$. These can be further quantified in terms of a nonvanishing octupole harmonic of the azimuthal distribution. Even though the predicted v_3 is small, on the order of v_4, it may be measurable at RHIC II [29].

The long range in rapidity $\Delta\eta \sim 4$–6 correlations induced by twisted sQGP initial conditions are expected to persist even at LHC energies, because the dimensionless parameter, $\delta \sim A^{1/3}/\log(s)$, that controls this phenomenon depends on the logarithm of the collision energy. Logarithms are very slowly varying functions of the energy, and thus the rate of reduction in δ with energy will be concomitantly slow.

ACKNOWLEDGMENTS

Discussions with J. Harris, T. Hirano, W. Horowitz, M. Lisa, I. Vitev, and X. N. Wang are gratefully acknowledged. This work is supported in part by the U.S. Department of Energy under Grant No. DE-FG02-93ER40764.

[1] K. Adcox *et al*. (PHENIX Collaboration), Nucl. Phys. A (to be published); B. B. Back *et al*. (PHOBOS Collaboration), arXiv:nucl-ex/0410022; I. Arsene *et al*. (BRAHMS Collaboration), arXiv:nucl-ex/0410020; J. Adams *et al*. (STAR Collaboration), Nucl. Phys. A (to be published); http://www.bnl.gov/bnlweb/pubaf/pr/ PR_display.asp?prID=05-38

[2] M. Gyulassy and L. McLerran, Nucl. Phys. **A750**, 30 (2005); See also articles by T. D. Lee, J. P. Blaizot, B. Muller, E. Shuryak, H. Stöcker, and X. N. Wang, Nucl. Phys. **A750**, 1–171 (2005); RBRC Workshop Talks on website http://www.bnl.gov/riken/May14-152004workshop.htm.

[3] M. Gyulassy, I. Vitev, X. N. Wang, and B. W. Zhang, in *Quark Gluon Plasma 3*, edited by R. C. Hwa and X. N. Wang (World Scientific, Singapore, 2003) p. 123–191; A. Kovner and U. A. Wiedemann, *ibid.* p. 192–248; P. Jacobs and X. N. Wang, Prog. Part. Nucl. Phys. **54**, 443 (2005).

[4] J. D. Bjorken, Phys. Rev. D **27**, 140 (1983).

[5] B. B. Back *et al*. (PHOBOS Collaboration), Phys. Rev. Lett. **94**, 122303 (2005).

[6] (STAR Collaboration), Phys. Rev. C (to be published).

[7] T. Hirano, Phys. Rev. C **65**, 011901(R) (2001); U. Heinz and P. Kolb, J. Phys. G. **30**, S1229 (2004).

[8] T. Hirano and Y. Nara, Nucl. Phys. **A743**, 305 (2004).

[9] V. K. Magas, L. P. Csernai, and D. Strottman, Nucl. Phys. **A712**, 167 (2002).

[10] W. Busza, Acta Phys. Polon. B **35**, 2873 (2004).

[11] A. Bialas, M. Blezynsky, W. Czyz, Nucl. Phys. **111**, 461 (1976); N. N. Nikolaev and S. Pokorski, Phys. Lett. **B80**, 290 (1979); Sov. Phys. Usp. **24**, 531 (1981) [Usp. Fiz. Nauk **134**, 369 (1981)].

[12] B. B. Back *et al*. (PHOBOS Collaboration), Phys. Rev. Lett. (to be published).

[13] G. J. Alner *et al*. (UA5 Collaboration), Z. Phys. C **33**, 1 (1986).

[14] X. N. Wang and M. Gyulassy, Phys. Rev. D **44**, 3501 (1991).

[15] M. Gyulassy and X. N. Wang, Comput. Phys. Commun. **83**, 307 (1994).

[16] S. J. Brodsky, J. F. Gunion, and J. H. Kuhn, Phys. Rev. Lett. **39**, 1120 (1977).

[17] B. Andersson, G. Gustafson, and B. Nilsson-Almqvist, Nucl. Phys. **B281**, 289 (1987).

[18] X. N. Wang, Phys. Lett. **B565**, 116 (2003).

[19] D. Kharzeev, E. Levin, and M. Nardi, Nucl. Phys. **A730**, 448 (2004); **A743**, 329(E) (2004).

[20] L. McLerran and R. Venugopalan, Phys. Rev. D **49**, 2233 (1994).

[21] I. Arsene *et al*. (BRAHMS Collaboration), Phys. Rev. Lett. **93**, 242303 (2004).

[22] A. Accardi and M. Gyulassy, Phys. Lett. **B586**, 244 (2004).

[23] W. D. Myers, Nucl. Phys. **A296** 177 (1978).

[24] Z. T. Liang and X. N. Wang, Phys. Rev. Lett. **94**, 102301 (2005).

[25] (BRAHMS Collaboration), Phys. Rev. Lett. 94, 162301 (2005).

[26] M. Gyulassy, I. Vitev, and X. N. Wang, Phys. Rev. Lett. **86**, 2537 (2001); M. Gyulassy, I. Vitev, X. N. Wang, and P. Huovinen, Phys. Lett. **B526**, 301 (2002).

[27] F. Retiere and M. A. Lisa, Phys. Rev. C **70**, 044907 (2004); J. Adams *et al*. (STAR Collaboration), Phys. Rev. Lett. **92**, 062301 (2004).

[28] A. Drees, H. Feng, and J. Jia, Phys. Rev. C **71**, 034904 (2005).

[29] J. Harris *et al*., Second RHIC II Science Workshop, http://www.bnl.gov/physics/rhicIIscience/; P. Steinberg *et al*., arXiv:nucl-ex/0503002.